The potential impacts of a sulfur- and halogen-rich super eruption such as Los Chocoyos on the atmosphere and climate

Hans Brenna[1], Steffen Kutterolf[2], Michael J. Mills[3], Kirstin Krüger[1]

[1]Section for Meteorology and Oceanography, Department of Geosciences, University of Oslo, P.O. Box 1022 Blindern, 0315, Oslo, Norway.
[2]GEOMAR | Helmholtz Centre for Ocean Research Kiel, Wischhofstrasse 1-3, 24148, Kiel, Germany
[3]Atmospheric Chemistry Observations & Modeling Laboratory, National Center for Atmospheric Research, P.O. Box 3000, Boulder, Colorado 80307-3000, USA

Correspondence to: Kirstin Krüger (kkrueger@geo.uio.no)

Abstract. The super-eruption of Los Chocoyos (14.6°N, 91.2°W), ~84 kyrs ago, in Guatemala was one of the largest volcanic events of the past 100,000 years. Recent petrologic data show that the eruption released very large amounts of climate-relevant sulfur and ozone destroying chlorine and bromine gases (523±94 Mt sulfur, 1200±156 Mt chlorine and 2±0.46 Mt bromine). Using the Earth System Model (ESM) CESM2(WACCM6) we simulate the impacts of the sulfur- and halogen-rich Los Chocoyos eruption on the pre-industrial Earth System.

Our simulations show that elevated sulfate burden and aerosol optical depth (AOD) persists for five years in the model, while the volcanic halogens stay elevated for nearly 15 years. As a consequence the eruption leads to a collapse of the ozone layer with global mean column ozone values dropping to 50 DU (80% decrease) leading to a 550% increase in surface UV over the first five years, with potential impacts on the biosphere. The volcanic eruption shows an asymmetric hemispheric response with enhanced aerosol, ozone, UV, and climate signals over the Northern Hemisphere. Surface climate is impacted globally due to peak AOD of >6 leading to a maximum surface cooling of >6 K, precipitation and terrestrial net primary production (NPP) decreases of >25%, and sea ice area increases of 40% in the first three years. Locally, a wetting (>100%) and strong increase of NPP (>700%) over Northern Africa is simulated in the first five years related to a southward shift of the Inter-Tropical Convergence Zone (ITCZ) to the southern tropics. The ocean responds with pronounced El Niño conditions in the first three years shifted to the southern tropics, coherent with the ITCZ change.

Recovery to pre-eruption ozone levels and climate takes 15 and 30 years respectively. The long-lasting surface cooling is sustained by an immediate increase in Arctic sea ice area, followed by a decrease of poleward ocean heat transport at 60° N lasting up to 20 years.

In contrast, when simulating Los Chocoyos conventionally, including sulfur and neglecting halogens, we simulate larger sulfate burden and AOD, more pronounced surface climate changes and an increase of column ozone. Comparing our aerosol chemistry ESM results to other super-eruption simulations with aerosol climate models we find a higher surface climate impact per injected sulfur amount than previous studies for our different sets of model experiments, since

CESM2(WACCM6) creates smaller aerosols with a longer lifetime partly due to the interactive aerosol chemistry. As the model uncertainties for the climate response to super eruptions are very large, observational evidence from paleo archives and a coordinated model intercomparison would help to improve our understanding of the climate and environment response.

1 Introduction

The Los Chocoyos (LCY, 14.6°N, 91.2°W) super-eruption (Kutterolf et al., 2016) of magnitude M=8 (calculated after Pyle, 2013), dated to ~84 kyrs before present (Rose et al., 1999), is known to be one of the largest volcanic eruptions of the past 100,000 years (Drexler et al., 1980). The eruption formed the current stage of the large Atitlán caldera in present-day Guatemala. LCY released more than ~1100 km^3 of tephra and the eruption is used as a widespread key stratigraphic marker during that time (Cisneros et al., in review; Kutterolf et al., 2016). The ash layers can be found in marine deposits from offshore Ecuador to Florida over an area of more than 10^7 km^2 (Kutterolf et al., 2016). Hardly anything is known about the climate impacts of this eruption from proxy records, but LCY emitted large amounts of climate and environmentally relevant gases including sulfur, chlorine and bromine compounds (Krüger et al., 2015; Kutterolf et al., 2015, 2016; Metzner et al., 2014).

The sulfur gases emitted by volcanoes have a strong direct climate impact through the formation of sulfuric acid aerosols which block incoming sunlight and cool the surface (Robock, 2000). Halogen compounds, such as chlorine and bromine, contribute to catalytic ozone depletion in the stratosphere (Brasseur and Solomon, 2005; Solomon, 1999). There is well-documented petrological evidence that volcanic super-eruptions have emitted environmentally significant amounts of chlorine and bromine (Cadoux et al., 2015, 2018; Krüger et al., 2015; Kutterolf et al., 2013, 2015; Vidal et al., 2016). Furthermore, recent atmospheric observations revealed that even relatively small volcanic eruptions can inject significant amounts of halogen compounds in the stratosphere (for review and overview discussions see von Glasow et al. (2009), Krüger et al. (2015) and WMO, (2018)). This means that a sulfur-and-halogen-rich eruption is expected to cool the Earth's surface and potentially damage the stratospheric ozone layer, with further impacts on the surface environment through the change in the atmosphere's transparency to harmful ultraviolet (UV), particularly shortwave UV-B, radiation (i.e. Brenna et al., 2019). Potential volcanic iodine injections to the stratosphere (Schönhardt, et al. 2017) would have even a larger ozone depletion potential than chlorine and bromine (Solomon, et al 1994). However, no direct iodine erupted mass measurements are available for the LCY eruption.

Metzner et al. (2014) used the General Circulation Model (GCM) MAECHAM5-HAM coupled with a modal aerosol microphysics scheme, together with the Earth System Model of Intermediate Complexity CLIMBER-2 to study the climate impact of LCY. Based on the former published mass estimate of 687 Mt SO_2 (343.5 Mt S), they simulated a peak cooling of 3.1°C from their LCY eruption scenario. Toohey et al. (2011, 2013) investigated atmospheric physical processes of LCY, using 700 Mt SO_2 (350 Mt S) injections with the model MAECHAM5-HAM, revealing the important effects of different

seasons of that eruption on the aerosol evolution, transport, and deposition of sulfate to the ice cores and compared them to weaker eruptions strengths.

Even though there is little literature about LCY, the climate impact of super-eruptions has been discussed in the scientific literature since at least the early 1990s. Early studies argued that the eruption of Toba (73 kyrs ago) could have initiated a glacial period (Rampino and Self, 1992, 1993; Zielinski et al., 1996). In addition, there is evidence that human populations went through a genetic bottleneck (i.e., most of the population died) at approximately the same time as the eruption of Toba (Ambrose, 1998; Haslam and Petraglia, 2010; Williams et al., 2009), but this is now considered unlikely (Timmreck et al., 2010, 2012).

A thorough investigation of the climatic and environmental impacts of extremely large to super volcanic eruptions (M: 7-8) requires the use of a global climate model or, ideally, an Earth System Model (ESMs). There are several studies published with different model complexities, mostly focusing on the Toba eruption and its sulfur impact on the atmosphere and climate.

Bekki et al. (1996) used a two-dimensional chemistry transport model with internally generated atmospheric circulation to study the Toba eruption impact on the atmosphere. Their simulations indicate that Toba could have caused a long-lasting atmospheric response due to the interactions between chemistry and aerosol microphysics.

Later, Jones et al. (2005) used a coupled atmosphere-ocean general circulation model (AOGCM) to study the Toba eruption impact on climate. In this study they forced the model by linearly scaling the observed aerosol optical depth (AOD) from the 1991 eruption of Mt. Pinatubo by a factor of 100, resulting in peak cooling of ~11 K in the 2nd post-eruption year, followed by an initial recovery taking a decade. Surface cooling larger than 1 K persisted for more than 20 years. The volcanic aerosol forcing only lasted 5 years, so the response needed to be maintained by feedbacks in other components of the Earth System through, i.e., sea-ice/ocean feedbacks sustaining the short atmospheric forcing to longer (decadal to centennial) time scales (Miller et al., 2012; Stenchikov et al., 2009; Zhong et al., 2011).

In a similar study, Robock et al. (2009) used three different AOGCMs to study the Toba eruption effect on climate and ozone. In their study, both the linear scaling AOD approach and directly injecting sulfur into a model with an interactive bulk aerosol module were utilized. The resulting magnitude and length of the cooling was similar to what was published in Jones et al. (2005) across the different model versions and forcing methods. The scenarios representing a 100 times Pinatubo forcing resulted in ~12 K peak cooling with multi-decadal recovery times. In a 300 times Pinatubo scenario simulation including atmospheric chemistry effects, Robock et al. (2009) found slightly stronger (~1 K) and much more long-lasting surface cooling (length of >10 K cooling extended by ~5 years) compared to the similar forcing scenario without chemistry, due to depletion of atmospheric hydroxyl (OH) limiting the speed of aerosol formation, leading to a longer-lasting forcing. In addition, they simulated an increase in global column ozone, attributed to the reduction of reactive hydrogen oxides in the atmosphere.

Another model study of Toba, presented in Timmreck et al. (2010, 2012) and Zanchettin et al. (2014), simulated a smaller climate impact with peak cooling of 3.5 K lasting up to 10 years from injected sulfur compared to the analogous simulations

in Robock et al. (2009). A key difference between Timmreck et al. (2010) and previous AOGCM simulations of Toba is the inclusion of online aerosol microphysics in a modal aerosol scheme and the OH limitation mechanism, leading to larger aerosol sizes, lower peak AOD (~4) values and thus lower climate impacts in Timmreck et al. (2010). The inclusion of interactive OH chemistry in the formation of aerosol is important because the availability of OH controls the speed of SO_2 oxidation into sulfate (Bekki, 1995).

Concentrating on the atmospheric processes, English et al. (2013) used a sectional aerosol microphysical model coupled to a chemistry climate model with prescribed sea surface temperatures (SSTs) to study the aerosols and atmospheric impacts of the Toba eruption. In their model setup, neglecting aerosol radiative effects, they simulate even lower peak AOD values (~2.6) due to the fact that their sectional aerosol module creates larger aerosols compared to Timmreck et al. (2010).

In the climate modeling literature on the Toba super eruption there is a progression from larger to smaller climate (and environmental) impacts as model complexity develops over time. In the more recent climate models one key reason seems to be that climate effects are self-limiting for larger eruptions due to an increase of aerosol growth which reduces peak AOD (English et al., 2013; Pinto et al., 1989; Timmreck et al., 2010). In addition, the role of atmospheric chemistry and OH limitation on sulfuric acid aerosols is continuously under discussion in the literature (Bekki, 1995; Mills et al., 2017; Niemeier et al., 2019; Robock et al., 2009; Timmreck et al., 2003).

Investigating the effects of the Toba eruption on the earth system such as hydrology and terrestrial net primary production (NPP) reveals a substantial reduction of precipitation globally leading to reduction of tree cover, increase of grass cover and decreased NPP, but with large regional and inter-model variability (Robock et al., 2009; Timmreck et al., 2010, 2012). While tropical deciduous trees and broadleaf evergreen trees virtually disappear in the simulations of Robock et al. (2009), Timmreck et al. (2011) find much more muted impacts on tree cover, particularly in the Tropics. Timmreck et al. (2011) even simulate an increase of NPP in the tropical rain forest regions of South America and Africa.

Recent studies proposed a sea ice/ocean mechanism which prolong the volcanic induced short, abrupt surface cooling and sea ice increase to longer time scales (decadal) with the ocean sustaining the signal by buffering and transporting the cooling poleward (Miller et al., 2012; Zhong et al., 2011). In addition, Zanchettin et al. (2014) simulated an interhemispheric response to different volcanic forcings with Pinatubo to Toba strength with Arctic sea ice expansion for all cases and an Antarctic sea ice expansion and subsequent contraction only for the super-eruptions.

We are not aware of studies of super-size eruption effects on the El Niño Southern Oscillation (ENSO), whereas the effects of large to very large (M: 5-6) volcanic eruptions have been widely discussed in the literature. There is an ongoing debate (Stevenson et al., 2017) that tropical volcanic eruptions can either lead to La Niña-like response in the same year (Anchukaitis et al., 2010; Li et al., 2013) or the following (five) years (Zanchettin et al., 2012) or to El Niño-like response up to the two following years (e.g., Adams et al., 2003; Handler, 1984; Khodri et al., 2017; Ohba et al., 2013; Predybaylo et al. 2017; Stevenson et al., 2016). Discussions include the significance and mechanism of the results as well as the eruption characteristics, latitude, season, and strength.

Simulations of halogen- (and sulfur-) rich eruptions show that these can have serious, long-lasting impacts on the ozone layer, with implications for the surface environment through the increase of surface ultraviolet radiation. In a 2D chemical transport model (CTM) study of the late Bronze Age eruption of Santorini (magnitude 7), Cadoux et al. (2015) simulated decadal ozone depletion, mainly in the northern hemisphere, with peak depletion of 20-90% depending on the degassing budget. In another study using a 2D CTM (Klobas et al., 2017), (hypothetical) volcanic halogens were included with the sulfur injection of Mt. Pinatubo, showing ozone depletion of 20% lasting a few years under different future emission scenarios. Using CESM1(WACCM) a comprehensive coupled chemistry climate model (CCM), with prescribed volcanic aerosols and SSTs, Brenna et al. (2019) simulated an average Central American Volcanic Arc (CAVA) eruption with magnitude 6.4. They found ozone depletion up to 20% globally lasting up to 10 years, which were most pronounced over the Northern Hemisphere (NH) and dropped below present-day ozone hole conditions over Antarctica and the tropics. Consequently, surface UV radiation increased by >80% over the 2 years with potential impacts on human health, agriculture and marine life.

We are not aware of super-eruption studies taking the combined effect of sulfur and halogen injections in a fully coupled aerosol-chemistry-climate ESM into account.

In this study we use the recently released CESM2 coupled with WACCM6 as the atmospheric component, which allows us to investigate newly the coupling and the feedbacks between volcanic aerosols, chemistry, radiation, climate and the earth system after a sulfur and halogen rich super volcanic eruption. The primary goal of this paper is to investigate the combined effect of the sulfur and halogen rich LCY super-eruption on climate and environment. In particular, we study the impacts of LCY by varying eruption composition and size on: i) atmospheric burden of volcanic gases and aerosols; ii) ozone and UV); iii) climate and environment; iv) ENSO. Finally, we compare with other model studies before we give a summary and conclusion. In a forthcoming paper, we will investigate the impacts on stratospheric circulation in the tropics.

2 Methods

2.1 Los Chocoyos eruption volatile estimates

Using the recently published total erupted mass estimate for the LCY eruption (Kutterolf et al., 2016) and the previously published petrologic estimates of volatile concentrations for sulfur, chlorine and bromine (Metzner et al., 2014; Kutterolf et al., 2013, 2015) we calculate a new mass of erupted volatiles for LCY as a starting point for defining the stratospheric injections in our model simulations. The erupted volatile masses as calculated using these estimates (+/- uncertainties) are 523±94 Mt sulfur (S), 1200±156 Mt chlorine (Cl) and 2±0.46 Mt bromine (Br).

The determination of volatile injection into the stratosphere during the LCY eruption is based on a two-step approach: The first step is the determination of erupted magma mass. LCY fall deposits are well exposed on land and within sediment and lacustrine cores on the Pacific seafloor as well as Lake Péten Itzá to create isopach (thickness) maps (Kutterolf et al. 2008a, 2016; Cisneros et al. in review). These maps serve as a basis to determine erupted total tephra volume by fitting straight lines

to data on plots of ln [isopach thickness] versus square root [isopach area] following Pyle (1989) and Fierstein and Nathenson (1992) and integrating to infinity as described in Kutterolf et al. (2016, 2008b, 2007). Additionally, outcrops identified in the field, in satellite images, and Google Earth, have been used to document regional thickness variations and finally to determine the volume of the flow deposits by integrating the results of different calculation methods (Cisneros et al. in review). We then converted tephra volume to magma mass following the procedure of Kutterolf et al. (2008b, 2016) by using variable tephra densities from proximal to distal deposits.

The second step is the measurement of volatile contents in both melt inclusion and matrix glasses (see Metzner et al. 2014, Kutterolf et al., 2015). Applying the petrological method (Devine et al., 1984), matrix glass represents the degassed melt after eruption and melt inclusion glass represent the volatile content prior the eruption. The concentration difference between melt-inclusion and matrix glasses yields the volatile fraction degassed during an eruption, and multiplication with erupted magma mass gives the mass of emitted volatiles (e.g. Kutterolf et al. 2015).

Both procedure steps are taken into account in the maximum combined uncertainty for the volatile budget of each volatile, which is ±13% for chlorine, ±18% for sulfur, and ±23% (see also Brenna et al. 2019).

Finally, the petrological method might underestimate the volcanic emission due to pre-eruptive, magma fluid partitioning by a factor of 10 for sulfur (Self and King, 1996) and a factor of 2 or more for halogens (Kutterolf et al 2015) as discussed earlier (Metzner et al 2014, Krüger et al 2015; Brenna et al 2019).

2.2 CESM2(WACCM)

In this study we use the Community Earth System Model Version 2 (CESM2) (Danabasoglu et al., in review) coupled with the Whole Atmosphere Community Climate Model Version 6 (WACCM6) (Gettelman et al., 2019) as the atmospheric component. CESM2(WACCM6) is a comprehensive numerical model spanning the whole atmosphere from the surface to the lower thermosphere with model top at ~140 km altitude. The chemistry module includes the SOx, Ox, NOx, HOx, ClOx and BrOx chemical families, implementing 98 compounds and ~300 reactions. It covers gas-phase, photolytic and heterogeneous reactions on three types of aerosols including polar stratospheric clouds which form interactively in the model. Stratospheric sulfuric acid aerosols are formed interactively from sulfur compounds and modeled by the modal aerosol model MAM4 (Liu et al., 2016), which has been adapted and extended for the stratosphere (Mills et al., 2016). CESM2(WACCM6), as a coupled CCM, allows us to explore the coupling between radiation, temperature, circulation, chemistry and composition in the atmosphere. The horizontal resolution is 0.95° longitude by 1.25° latitude with 70 hybrid sigma pressure layers from the surface to 5.5×10^{-6} hPa (approximately 140 km altitude). The quasi-biennial oscillation (QBO) is internally generated and has a period of ~27 months, which is close to observations (Gettelman et al., 2019). However, the QBO amplitude is too weak and the oscillation does not extend into the lowermost stratosphere, which can impact QBO teleconnections to the extratropics.

The ocean model of CESM2(WACCM6) is the Parallel Ocean Project v. 2 (POP2) model running at ~1°×1° horizontal resolution with 60 layers in the vertical. CICE5 is the sea ice model for CESM2(WACCM6) (Bailey et al., 2018) which is

running on the same grid as POP2. The land surface model in CESM2(WACCM6) is the community land model Version 5 (CLM5) set up under 1850 conditions with dynamic vegetation, interactive biogeochemistry (carbon, nitrogen, methane) and prognostic crops (Fisher et al., 2019).

2.3 Model experiments

To model the impact of the LCY eruption on the atmosphere we use the petrological estimated erupted sulfur and halogen masses as input. We inject all 523 Mt of the erupted sulfur mass as 1046 Mt of SO_2. For the volcanic halogens we inject only 10% of the estimated erupted halogen mass into the stratosphere as HCl and HBr, and assume that the rest is removed before reaching the stratosphere. We consider this a reasonably conservative estimate for halogen injection efficiency based on observations and simulations of volcanic plumes, yielding ranges from 2-25% (see further discussions in Brenna et al. 2019 and Krüger et al. 2015). The volcanic volatiles are injected into the model grid boxes at 14.6°N and between 80° and 97.5°W, at 24 km altitude. The eruption date is set to January, since the eruption season is not known. Injecting this huge amount of mass over one time step in a single grid box was not possible due to model stability. Thus, spreading the injection over longitude (80°-97.5° W) and time (1-6 January) was chosen as a model experiment compromise. We run the LCY Atitlán super-eruption model experiments under 1850 pre-industrial conditions, which was the closest available model set up to paleoclimate conditions.

We run an ensemble of six simulations for the combined sulfur and halogen forcings (**LCY_full**) starting from different ENSO (positive, negative, neutral) and QBO (easterly, westerly) states of the control simulation (**Ctr**), which is a single 70 year simulation with constant 1850 forcings. In addition, we perform two simulations (QBO easterly and westerly, ENSO neutral, branching from the same **Ctr** years as for **LCY_full**) with only the sulfur forcing (**LCY_sulf**) to explore the difference in response between the forcing scenarios. All ensemble members last 35 years. In all simulations, background stratospheric concentrations of chlorine and bromine are 0.45 ppbv and 10.2 pptv at the 10 hPa level respectively, consistent with preindustrial estimates (WMO, 2014). In addition to these main experiments, we have performed two sensitivity simulations. One with sulfur injection reduced by a factor of 100 (**LCY_1%sulf**) and one with full sulfur injection and 1% halogen injection efficiency instead of 10% (**LCY_1%halog**). The experiments are summarized in Table 1.

2.4 Surface UV calculations

We calculate the UV radiation at the surface using the Tropospheric Ultraviolet and Visible (TUV) radiation transport model (Madronich and Flocke, 1997) using similar methods as in Brenna et al. (2019). In our setup, TUV solves the radiative transfer equations given the parameters: Date of the year, position, time of day, column ozone values and total AOD at 550 nm taking aerosol scattering into account. We run the TUV model offline for each point in latitude and longitude and using hourly temporal resolution to get a representation of the variations in UV throughout the year. As input to the TUV model we give averages of column ozone and AOD over the first five years after the eruption for LCY_full and LCY_sulf and for the control run to generate UV fields for the eruption scenarios and for the control run climatology.

2.5 Oceanic Niño Index (ONI)

To select initial conditions for the set-up of the ensembles and to quantify the impact of the volcanic eruptions on the ENSO we calculate the Oceanic Niño Index (ONI) from the model output. The ONI index is used operationally by NOAA to analyze the ENSO state (https://origin.cpc.ncep.noaa.gov/products/analysis_monitoring/ensostuff/ONI_v5.php). To calculate the index, the average SST anomalies in the Nino3.4 region (5° N-5° S, 120°-170° W) are filtered using a 3-month running mean based on centered 30-year periods. If this index is above or below 0.5 K for at least 5 consecutive months, we have an El Niño or La Niña respectively.

For our study we used the full control simulation as the baseline. As the large temperature response caused by the simulated LCY eruption masks the ENSO response initiated by the eruption, we have used relative sea surface temperature anomalies (RSSTAs) instead of the SST anomalies following Khodri et al. (2017). The RSSTA is calculated by removing the tropical mean (20°S – 20°N) SST anomaly from the SST anomaly at every point. This quantity better isolates the intrinsic ENSO signal than standard SST anomalies (Khodri et al. 2017).

3 Results and discussion

3.1 Atmospheric burdens of volcanic gases and aerosols

Using our modeling approach results in the atmospheric burdens of volcanic gases and aerosol as summarized in Figure 1. To compare the decay time of the volcanic perturbations of sulfur and halogens between the different eruption scenarios, we calculated normalized burden anomalies in addition to standard anomalies. For this, we divided the burden anomalies in each scenario with the maximum burden anomalies in that scenario, providing normalized values between one and zero. The normalized total sulfur burden after the simulated eruptions has an e-folding time (reduction by 1/e) of a little more than two years (Figure 1b). There is first a plateau for ~1 year before decay starts. The following e-folding times ($1/e^2$ and $1/e^3$) are shorter, a bit less than 1 year. After ~5 years nearly all of the sulfur has been removed from the atmosphere. The total sulfur burden lifetimes are remarkably similar for all four injection scenarios, even when the injection amounts differ by a factor of 100. In contrast, the halogens have a longer first e-folding time of approximately 3 years, but the following e-folding times are ~1 year, similar to what we simulate for total sulfur. After ~15 years nearly all of the halogens have been removed from the atmosphere (not shown here).

The conversion of injected SO_2 into sulfuric acid aerosol is significantly slowed down in the LCY_sulf, LCY_full and LCY_1%halog scenarios compared to the LCY_1%sulf, where we only injected 1% of the sulfur (Figure 1 d). The e-folding time of the SO_2 burden increases from ~3 months to ~6 months when the injected SO_2 mass is increased by a factor of 100. There is an additional increase in lifetime to ~1 year when halogens are injected in addition to SO_2. This increase in SO_2 lifetime is caused by the limited oxidizing capacity of the atmosphere (see also Bekki et al. 1995). The main compound responsible for oxidizing SO_2 to sulfuric acid is OH. When the SO_2 burden increases the availability of OH is limited and

oxidation slows down. When halogens are injected in addition, reactions involving halogens also consume OH (Figure 1f) further limiting the OH available for SO_2 oxidation, and thus further increasing the SO_2 lifetime (Fig. 1d). This OH depletion effect may be partly offset by an increase of water vapour and hence HOx into the stratosphere due to the volcanic aerosol heating of the tropical tropopause. However, as the tropical tropopause layer is warmed from 6 month up to year 3 after the eruption (not shown here), we evaluate this effect to play a minor role during the first half year after the eruption when the SO_2 conversion mainly takes place.

The peak aerosol mass, when the sulfur burden is the same, depends on the conversion time of SO_2 into aerosol. Thus, the peak aerosol mass is lower in the LCY_full scenario compared to the LCY_sulf (Figure 1c). Even though the peak burdens are different, the lifetime of the aerosol mass perturbation is very similar in the two cases (Figure 1d), indicating that the removal mechanisms in these scenarios are very similar. The global mean weighted aerosol effective radius is very similar in these two scenarios, while in the LCY_1%sulf the aerosols have much smaller effective radii (factor ~3.5 smaller) (Figure 1e), as expected when the injection is smaller (English et al., 2013; Pinto et al., 1989; Timmreck et al., 2010). After the eruption of Pinatubo, aerosol radii were estimated to be approximately 0.5 μm (Russel et al., 1996), compared to 0.2 μm for our LCY_1%sulf scenario and 0.7 μm for the other scenarios, which might indicate that the aerosols are too small in our model. Even though the aerosols are smaller in the LCY_1%sulf simulation, the removal time scale for the aerosols is similar to the two other scenarios. This indicates that gravitational settling is playing a minor role as removal mechanism for the aerosol mass in this model, and removal processes are happening on the transport time-scale of the stratosphere

Since the maximum aerosol mass in the LCY_sulf is ~25% larger compared to the maximum mass in LCY_full, while the aerosol sizes are approximately the same, we find that the peak AOD at 550 nm is larger in the LCY_sulf (>8) compared to the LCY_full scenario (~6) (Figure 2a). This translates into a larger energy imbalance at the top of the model in LCY_sulf (Figure 2b). The maximum radiative imbalance at the top of the model is approximately -50 W/m^2 in the LCY_sulf and -40 W/m^2 in the LCY_full scenario. In both cases, an initial strong negative net imbalance is followed by a small positive net imbalance after ~3.5 years, and throughout the climate recovery period.

3.2 Ozone and UV response

Global ozone collapses after the eruption in the LCY_full scenario, with whole column values decreasing by >80% to a global mean value of 50 DU during years 2-3 after the eruption (Figure 3a). Ozone levels lower than present-day Antarctic ozone hole conditions (<220 DU) persist for 8 years over the whole globe (Figure 3a, S1). Depletion shows a bi-modal distribution in the stratosphere, with maximum depletion in the upper (~4 hPa) and lower (~30 hPa) stratosphere (Figure S2). In the lower stratosphere, where most of the ozone mass is located, >70% of ozone is destroyed after 1 year, and this level of depletion persists for 7 years (not shown). Peak depletion in the lower stratosphere is >95%. Significant global mean ozone column reduction lasts for ~12 years. In the Antarctic, ozone hole conditions continue re-occurring annually for 15 years (Figure S1b). Compared to LCY_full, the ozone response in LCY_1%halog is smaller, but reveals a similar response. A substantial decrease to global mean column values of ~150 DU and a recovery after about 10 years; a larger and longer

lasting ozone response as was simulated for an average CAVA eruption with M=6 and 10% halogen injection efficiency (Brenna et al. 2019).

In contrast, in the LCY_sulf scenario, the column ozone increases by more than 100 DU in the first year after the eruption (Figure 3a). This is caused by the increase in heterogeneous chemistry taking place on the sulfate aerosols which reduces the concentrations of ozone-destroying NO_X (Tie and Brasseur, 1995) and was modelled for very large and super volcanic eruptions injecting sulfur into a pre-industrial stratosphere with low chlorine background levels (Muthers et al., 2015; Robock et al., 2009). The ozone increase decays in about 3 years and is only slightly elevated after that until post-eruption year 10 (Figure 3a). The increase in ozone is concentrated in the mid to high latitudes and mostly in the NH (Figure S1c).

In Figure 4 we present global maps of total AOD (a,b), as well as anomalies and the climatologies for column ozone and surface UV (g,h) averaged over the first five years (referred to as pentadal) after the eruption for both the LCY_full and LCY_sulf scenarios. The spatial pattern in AOD is similar between the LCY_full and LCY_sulf scenarios with larger AOD anomalies in the extratropics compared to a band of low AOD in the Southern Hemisphere (SH) tropics, and the largest impacts in the NH (Figure 4 a, b). In LCY_full, AODs are smaller over Antarctica than at lower latitudes. This might be because transport to the Antarctic region is suppressed by the strengthening of the Westerlies winds surrounding the southern polar vortex (not shown here), which acts as a transport barrier for very large eruptions (Toohey et al., 2013). In LCY_sulf the global mean AOD is larger (c.f. Figure 2a), which holds for the local distribution over the globe as well (Figure 4a, b).

Figure 4g and h shows the calculated change in the amount of surface ultraviolet radiation (UV-B) weighted for DNA damage calculated using the radiation transport model TUV (see Methods). Taking into account both the change in AOD and the change in column ozone in the TUV calculations we find very large, but opposite signals in the two eruption scenarios. In the LCY_full scenario, the largest increases in surface UV are more than 1400% in the Arctic and more than 1000% in the Antarctic. Changes are generally smaller towards the equator, but no part of the planet experiences less than a 200% increase. Global average UV increase over the five-year period is 545%. By contrast, in the LCY_sulf scenario the UV-B decreases by more than 80% in the mid-to-high latitudes of the NH and by >60% over most of the rest of the planet (Figure 4g,h). The UV response in our calculations are impacted by the ozone levels and the AOD (Figure 4a-f), and in LCY_full the AOD and ozone effects are opposing each other with the ozone effects being strongest, while in LCY_sulf they are both contributing to a decrease in surface UV.

3.3 Climate and environmental response

3.3.1 Global surface temperature decreases for 30 years

Time series of global mean surface temperatures are shown in Figure 3b. For both scenarios, global mean surface temperature decreases more than 6 K and returns to climatological background after approximately 30 years. The peak cooling in year 2 for LCY_sulf is more than 1 K greater than that for LCY_full. If the aerosol response from the sulfur injection (which is the same in these two scenarios) were the same, we would expect the temperature response to be very

similar. Instead, we interpret this difference in surface temperature response due to the large difference in peak AOD (Figure 2a).

In Figure 5 (a, b) we show maps of surface temperature anomalies averaged over the first five post-eruption years for the scenario LCY_full and the difference to LCY_sulf; LCY_sulf is added to the supplement (Figure S3a). Higher surface temperatures in LCY_full than LCY_sulf cover almost the whole globe except polar regions, which might be slightly cooler since ozone depletion in the stratosphere is a negative radiative forcing on the global climate system (Myhre et al., 2013). Temperature anomaly patterns are relatively similar between the scenarios with surface cooling almost globally and largest anomalies in the NH and over the continents. The magnitudes are large (larger in LCY_sulf, c.f. Figure 3b), even in a five year mean, with most continental areas experiencing at least 4 K cooling, locally dropping <10 K over central Asia (Figures 5a,b; S3a).

3.3.2 Sea-ice/ocean changes for 20 years

The long lasting global cooling response cannot be explained by the direct radiative forcing from the volcanic aerosols, since the aerosols have mostly disappeared after 5 years. In Figure 3c we show the 12 month running mean change in global mean sea ice area. Sea ice immediately response to the eruption induced surface cooling with a peak increase of sea ice area globally up to 40% in LCY_full and up to 50% in LCY_sulf. Global sea ice area in the model experiments is not back to climatological values before at least 20 years after the eruption. When inspecting NH sea ice and ocean changes more in detail (Figure S4) we find that Arctic sea ice area is increased immediately after the eruption and for more than 20 years with a maximum of 7 million km^2 (not shown), a 104% increase in post-eruption year 2. This change is accompanied by a reduction of ocean heat content (not shown) and a decrease of poleward ocean heat transport at 60°N after the eruption, lasting from post-eruption year 3 up to 20 with a maximum decrease up to 0.1 PW (20%) in post-eruption year 5 (Figure S4). Thus, abrupt surface cooling and decrease of upper ocean heat content in the NH leads to an immediate increase of Arctic sea ice area in the first years. The reduced poleward ocean heat transport at northern mid-latitudes for up to 20 years sustains the sea ice and climate surface cooling signal for more than 20 years in the NH and also globally. Antarctic sea ice area reveals an inter-hemispheric asymmetric response with slightly later and shorter lasting increase from post-eruption years 1 to 5 and in contrast to Zanchettin et al (2014) no subsequent contraction. The poleward ocean heat transport at 60°S is much more variable than in the NH and does not show significant changes over longer time periods in our simulations. This may be due to the later supply of AOD to the southern hemisphere (SH) (Figure S1), thus later radiative forcing, as well as smaller AOD and hence weaker surface climate response in the SH compared to the NH (Figures 4, and 5). For a tropical January eruption, AOD is first distributed in the tropical belt in the first few weeks before being transported poleward to the NH winter/spring season and then to the SH in the following months (Figure S1; see also Toohey et al., 2011), reflecting the pathways and seasonality of the Brewer Dobson circulation (Plumb, 2002). Atmospheric circulation changes are expected to be significant for the LCY eruption as was shown by Toohey et al. (2011, 2013).

3.3.3 Large impacts on precipitation and vegetation

A strong cooling of the atmosphere, like from an explosive volcanic eruption, leads to decreased precipitation (Robock and Liu, 1994). In our simulations, global mean precipitation (Figure 3d) decreases ~25% (~0.8 mm/day) in the LCY_full scenario and more than ~30% (1 mm/day) in the LCY_sulf scenario. The LCY_sulf simulation is outside the two standard deviation range of the LCY_full ensemble. Return to background climatological precipitation takes more than 10 years in both scenarios. The minimum precipitation is found between 2 and 3 years after the eruption, closely following the drop in the temperature signal.

Post-eruption pentadal precipitation patterns are shown in Figure 5 (c - f) for LCY_full and the difference to LCY_sulf; LCY_sulf is added to the supplement (Figure S3 (b, c)). Pentadal precipitation patterns are similar in both scenarios, with drying over approximately two thirds of the planet, a distinct southward shift of the Inter-Tropical Convergence Zone (ITCZ) in the Pacific and Atlantic to the SH tropics and wetting on the subtropical east sides of the oceanic basins. In addition, there is a pronounced wetting signal (>100%) throughout the tropical East Atlantic, Northern Africa, Middle East, and the Arabian Peninsula. These are relatively dry regions, so an absolute increase in precipitation (<1 mm/day) corresponds to more than a doubling of rainfall over large parts of this region. Comparing LCY_full and LCY_sulf, the impacts are generally weaker for the first scenario both where we find drying and wetting.

The strong AOD increase, global surface cooling, and decrease in precipitation together result in a decrease in land plant productivity (Net Primary Production (NPP) of >30% during the first three years after the eruption, followed by suppressed production during the next ~15 years in both scenarios (Figure 3e). NPP is especially reduced over the NH land with peak decrease >75% over high latitudes and a gradual weakening of this signal towards lower latitudes (Figures 5g,h, S3d, S5). However, over Northern Africa and surrounding areas, where precipitation increases significantly due to the southward shift of the ITCZ, we find a corresponding enhancement in land plant productivity as shown by a strong increase in NPP in this region. This is by far the strongest signal we detect in NPP with more than 400% gain in some areas. Comparing LCY_full and LCY_sulf, the NPP decrease is generally weaker for the first scenario for the global mean and also for most of the globe locally.

3.4 El Niño conditions

The ENSO response of the simulations is shown in Figure 6. Even though the initial conditions of the experimental set-up span different ENSO states, there is a rapid convergence to a robust response in the LCY_full eruption scenario. ONI RSSTA values increase above 2 K during the first three years after the eruption. The model ensemble spread is suppressed for five years after the eruption, before beginning to diverge again. The ONI values exceed the range of natural variability in the control simulation with two distinct maxima during post-eruption years 0 (September to November) and 1 (November to

January). The LCY_sulf and LCY_1%halog simulations reveal an even longer lasting strong El Niño response lasting into year 2 in accordance with the longer-lasting volcanic forcing (Figure 2).

Maps of RSSTA (Figure 6b) for LCY_full (and LCY_sulf not shown) depict a strong El Niño response shifted to the SH maximizing at 12°S coherent with the southward shift of the ITCZ (Figure 5).

This clearly shows that the simulated LCY eruption leads to pronounced El Niño conditions shifted to the SH tropics during the first three post-eruption years.

4. Comparison with other studies

Our simulations reveal very large climate impacts from the LCY sulfur- and halogen-rich super-eruption, which are larger than other recent simulation studies of super eruptions. In Figure 7 we show scatter plots comparing our simulations of LCY to other simulations of super volcanic eruptions using sulfur only injections (English et al., 2013; Jones et al., 2005; Metzner et al., 2014; Robock et al., 2009; Timmreck et al., 2010).

Compared to other model studies with interactive aerosols of volcanic eruptions of magnitude M > 7, our simulations show very large maximum AODs and thus maximum surface climate impacts for a given sulfur injection (Figure 7 a, b). The largest climate cooling for a super eruption is achieved when using linearly scaled AOD values based on Pinatubo (Jones et al., 2005; Robock et al., 2009), but this approach is simplified, since there are several feedbacks (i.e., self-limiting, scattering, and removal of aerosols) that makes the relationship between sulfur injection, aerosols, radiative forcing, and climate highly non-linear (i.e., Bekki, 1995; Metzner et al., 2014; Pinto et al., 1989).

Limiting our comparison to model studies that use sulfur injection to generate self-consistent AOD estimates, we see that our model experiments show longer aerosol life time, larger radiative impacts and larger surface cooling per injected sulfur mass to the stratosphere than those studies (English et al., 2013; Metzner et al., 2014; Timmreck et al., 2010). A model intercomparison for the Tambora eruption revealed that version 5 of WACCM also has the longest aerosol life time among compared models (Marshall et al., 2018). The differences (Figure 7) could be caused by different model top levels, aerosol microphysics (bulk vs. modal vs sectional modules), radiation, advection and depositions schemes (see discussions by English et al 2013 and Marshall et al. 2018), as well as atmospheric chemistry (OH, ozone, H_2O) and climate/ESM model differences (coupling, resolution, clouds). Our comparison is limited by the fact that the simulations were not part of a coordinated model intercomparison yet, thus the model experiments are all different related to eruption strength, date, location, and injection altitude. Volcanic aerosol climate model intercomparisons are in progress now (see Timmreck et al., 2018; Zanchettin et al., 2016) and should include extremely large to super-size eruptions, where the model spread is even larger (Figure 7) but observational evidence is lacking.

Even though the halogen injection efficiency for a super eruption like LCY is highly uncertain, we expect that the effects of injected halogens would be qualitatively similar independent of the magnitude of the injection as our model results for 10% and 1% halogen injections reveal. Injecting additional volcanic halogens into the stratosphere leads to ozone depletion (this

study; Brenna et al., 2019) and the interaction with the OH availability impacts the aerosol formation leading to smaller maximum AOD and hence weaker surface cooling. Including the volcanic release of halogens as well as sulfur should be part of future model intercomparisons focusing on volcanic impacts on climate and ozone.

Figure 7c shows a clear, nearly linear relationship between peak surface cooling and peak AOD. This is consistent with previous studies (Hansen et al., 1980; Metzner et al., 2014; Timmreck et al., 2012).

When atmospheric temperatures drop after a volcanic eruption, changes in energy balance of the climate system leads to decreased global mean precipitation (Iles et al., 2013; Robock and Liu, 1994). The global mean precipitation response to the super volcanic eruptions follows a nearly linear relation with temperature (Figure 7d), larger cooling leads to larger negative precipitation anomalies through a weakening of the global hydrological cycle since lower temperatures leads to lower relative humidity in the troposphere. Our modeled southward shift of the ITCZ towards the southern tropics is accompanied by increased precipitation across North Africa and the Middle East, which is partly simulated also in Robock et al. (2009) and Timmreck et al. (2010, 2012), but the area experiencing wetting is larger in our simulations. The wetting of North Africa and the Middle East in our simulations leads to a strong increase in NPP in this area and thus likely to a greening of the Sahara. Timmreck et al. (2012), with only half the volcanic forcing that we simulate, shows NPP maps (vegetation impacts are simulated using an off-line vegetation model), and here there is very little change over the first three post-eruption years throughout this region. While we cannot compare our NPP field directly to the changes in vegetation types presented in Robock et al. (2009), we note that they simulate an increase in grass cover throughout North Africa and parts of the Middle East where there is very low vegetation cover in their control run, which would imply an increase in NPP in this region as well.

We simulate pronounced El Niño conditions to our LCY super eruption during the first three post-eruption years, superposed on a strong surface cooling signal. El Niño conditions may be favored as discussed in more details by Emile-Geay et al. (2008) due to the uniform solar dimming leading to a thermostat mechanism (Clement et al., 1996) initiating air-sea interaction in the equatorial Pacific. Our simulations of the sulfur- and halogen-rich LCY super eruption in the Northern tropics (14.6° N) during January adds another puzzle piece to the ongoing discussion of volcanic eruption impacts on ENSO (see Introduction). A coordinated model intercomparison study would help to shed more light into the different model response and mechanism.

Atmospheric circulation changes at high latitudes (i.e., stratospheric polar vortices, Annular Modes) are expected to be significant as was investigated by Toohey et al. (2011, 2013). A follow-up LCY paper will investigate the impacts on the stratospheric circulation in the tropics, the QBO, in more detail.

Using a fully coupled ESM with interactive aerosols and atmospheric chemistry is currently the best possible way to simulate the impacts of super-volcanoes on the Earth system. Our model setup takes into account the interactive coupling between most of the components of the Earth system, including ocean, sea-ice, bio-geochemistry, land surface and vegetation interactions. In addition, the inclusion of interactive aerosols and atmospheric chemistry is crucial to correctly simulate the feedbacks between the chemical composition of the atmosphere, aerosols and radiation. That said, there is still

considerable uncertainty in the impacts of volcanic sulfur injections, particularly in the conversion of SO_2 into sulfate aerosol, aerosol size and the lifetime of the radiative perturbation. The uncertainty in the Earth system's reaction to a given volcanic aerosol radiative forcing seems to be smaller (c.f. Figure 7c). Two recent studies suggest that LCY might have been the eruption of the last 100 kyrs with the largest climate impact. Cisneros et al. (in review) report a new, higher, sulfur mass estimate for LCY. Meanwhile, Toba is estimated to be less sulfur-rich than previously assumed (Chesner and Luhr, 2010). To compare these two super-eruptions and petrological estimates, other archives such as ice core records would be needed. However, no tephra has been identified in Greenland and Antarctica ice cores for both eruptions up to now (Abbott et al., 2012; Svensson et al., 2013). This model study together with a new examination of the LCY eruption date and a higher mass estimate (Cisneros et al., in review) will hopefully stimulate upcoming studies finding corresponding paleo proxies in ice cores, climate, and archaeological archives with high temporal resolution and precision.

5. Summary and conclusions

We simulated the Los Chocoyos (LCY) eruption of Atitlán under 1850 pre-industrial conditions with 523 Mt sulfur, 1200 Mt chlorine, and 2 Mt bromine emissions, assuming 10% stratospheric injection efficiency for the halogens. The model results may have been similar for LCY 84.000 years ago, as we did not set up the simulations with observed initial conditions and there are uncertainties in volcanic emissions. As expected, if there are large halogen emissions, the climate and environment response is different than if the volcano only emits sulfur into the stratosphere. Overall, we evaluate our model results to show a lower estimate of the possible climate and environment response given the likely low estimates for our petrologically derived volcanic emissions.

Our comprehensive aerosol chemistry Earth System Model (ESM) study shows that a sulfur- and halogen-rich tropical super-eruption like LCY has massive impacts on global climate and the environment lasting at least 20-30 years.

In the model, enhanced volcanic sulfate burdens and aerosol optical depth (AOD) persists for five years, while the halogens stay elevated for ~14 years. Under pre-industrial conditions, the eruption leads to a global collapse of the ozone layer (80% decrease) with global mean values of 50 DU and increasing surface UV-B by 550% globally over the first five years after the eruption. (In high latitudes the increase is >1000%). The ozone layer takes 15 years to recover. The simulated volcanic eruption, at 14.6° N in January, shows an asymmetric hemispheric response with enhanced AOD, ozone, UV, and climate signals over the Northern Hemisphere (NH).

The eruption cools the global climate lasting more than 30 years with the peak AOD of >6 leading to surface cooling >6 K and precipitation and terrestrial net primary production (NPP) decreases up to 30% in the first two years. Locally, a wetting (>100%) and strong increase of NPP (>400%) over Northern Africa is simulated in the first five years related to a southward shift of the Inter-Tropical Convergence Zone (ITCZ) to the southern tropics. Global sea ice area almost doubles, and the long-lasting surface cooling is sustained by an increase in Arctic ice area, followed by a decrease of poleward ocean heat

transport at 60° N from year 3. Both changes lasting up to 20 years. The ocean responds with pronounced El-Niño conditions in the first three years maximizing at 12°S coherent with the southward shift of the ITCZ.

In contrast, simulations of LCY including sulfur, but neglecting halogens, reveal larger sulfate burden and maximum AOD (~8), hence a larger radiative forcing with more pronounced surface climate cooling (>7 K) and reduced precipitation (25%) globally, even though spatial patterns of changes are similar to the simulations including volcanic sulfur and halogens. The environmental impacts reveal the opposite signal with a short-lived increase of column ozone of 100 DU (>30%) and decrease of UV (>60%) lasting up to three years.

LCY is one of the largest volcanic eruptions over the past 100 kyrs and we predict large impacts on the biosphere and thus any human populations at that time. Finding paleo proxies showing the impact of LCY on climate and the environment should be possible, given the large long lasting impact from our ESM simulations, but will require high (sub-decadal) temporal-resolution archives using the eruption as a time marker.

6. Code and data availability

All simulation data will be archived in the Norwegian National e-Infrastructure for Research Data (NIRD) Research Data Archive on acceptance of the manuscript. Post processing and visualization of data was performed with Python and the code and post processed data files are available on request from the corresponding author.

7. Supplement

The supplement related to this article is available online at:

8. Author contributions

HB performed the simulations, data analysis and produced the figures. HB, KK and SK interpreted the results. MM provided the CESM2(WACCM6) model and supported HB in performing simulations. HB wrote the manuscript with contributions from all co-authors.

9. Competing interests

The authors declare that they have no conflict of interest.

10. Acknowledgements

The authors want to thank the CESM model team at NCAR for providing the CESM2(WACCM6) model code and for their technical model support. The simulations for this study were performed on resources provided by UNINETT Sigma2 - the National Infrastructure for High Performance Computing and Data Storage in Norway. The publication of this article is funded by the EGU through the 2018 Outstanding Student Poster and PICO Award for HB.

References

Abbott, P. M., Davies, S. M., Steffensen, J. P., Pearce, N. J. G., Bigler, M., Johnsen, S. J., Seierstad, I. K., Svensson, A. and Wastegård, S.: A detailed framework of Marine Isotope Stages 4 and 5 volcanic events recorded in two Greenland ice-cores, Quat. Sci. Rev., 36, 59–77, doi:10.1016/j.quascirev.2011.05.001, 2012.

Adams, J. B., Mann, M. E. and Ammann, C. M.: Proxy evidence for an El Niño-like response to volcanic forcing, Nature, 426(6964), 274–278, doi:10.1038/nature02101, 2003.

Ambrose, S. H.: Late Pleistocene human population bottlenecks, volcanic winter, and differentiation of modern humans, J. Hum. Evol., 34(6), 623–651, doi:10.1006/jhev.1998.0219, 1998.

Anchukaitis, K. J., Buckley, B. M., Cook, E. R., Cook, B. I., D'Arrigo, R. D. and Ammann, C. M.: Influence of volcanic eruptions on the climate of the Asian monsoon region, Geophys. Res. Lett., 37(22), doi:10.1029/2010GL044843, 2010.

Bailey, D., Hunke, E., DuVivier, A., Lipscomb, B., Bitz, C., Holland, M., Briegleb, B. and Schramm, J.: CESM CICE5 Users Guide. [online] Available from: https://buildmedia.readthedocs.org/media/pdf/cesmcice/latest/cesmcice.pdf, 2018.

Beerling, D. J., Harfoot, M., Lomax, B. and Pyle, J. a: The stability of the stratospheric ozone layer during the end-Permian eruption of the Siberian Traps., Philos. Trans. A. Math. Phys. Eng. Sci., 365(1856), 1843–66, doi:10.1098/rsta.2007.2046, 2007.

Bekki, S.: Oxidation of volcanic SO2: A sink for stratospheric OH and H2O, Geophys. Res. Lett., 22(8), 913–916, doi:10.1029/95GL00534, 1995.

Brasseur, G. P. and Solomon, S.: Aeronomy of the middle atmosphere: Chemistry and physics of the stratosphere and mesosphere, Planet. Space Sci., 644, doi:10.1016/0032-0633(85)90091-1, 2005.

Brenna, H., Kutterolf, S. and Krüger, K.: Global ozone depletion and increase of UV radiation caused by pre-industrial tropical volcanic eruptions, Sci. Rep., 9(1), 1–14, doi:10.1038/s41598-019-45630-0, 2019.

Cadoux, A., Scaillet, B., Bekki, S., Oppenheimer, C. and Druitt, T. H.: Stratospheric Ozone destruction by the Bronze-Age Minoan eruption (Santorini Volcano, Greece), Sci. Rep., 5(April), 12243, doi:10.1038/srep12243, 2015.

Cadoux, A., Iacono-Marziano, G., Scaillet, B., Aiuppa, A., Mather, T. A., Pyle, D. M., Deloule, E., Gennaro, E. and Paonita, A.: The role of melt composition on aqueous fluid vs. silicate melt partitioning of bromine in magmas, Earth Planet. Sci. Lett., 498, 450–463, doi:10.1016/j.epsl.2018.06.038, 2018.

Chesner, C. A. and Luhr, J. F.: A melt inclusion study of the Toba Tuffs, Sumatra, Indonesia, J. Volcanol. Geotherm. Res., 197(1–4), 259–278, doi:10.1016/j.jvolgeores.2010.06.001, 2010.

Cisneros de León, A., Schindlbeck-Belo, J. C., Kutterolf, S., Danišík, M., Schmitt, A., Freundt, A. and Pérez, W.: A history of violence: magma incubation, timing, and tephra distribution of the Los Chocoyos super-eruption (Atitlán Caldera, Guatemala), in review at Journal of Quaternary Science.

Clement, A. C., Seager, R., Cane, M. A. and Zebiak, S. E.: An ocean dynamical thermostat, J. Clim., 9(9), 2190–2196, doi:10.1175/1520-0442(1996)009<2190:AODT>2.0.CO;2, 1996.

Danabasoglu, G., Lamarque, J.-F., Bacmeister, J., Bailey, D. A., DuVivier, A. K., Edwards, J., Emmons, L., Fasullo, J., Garcia, R., Gettelman, A., Hannay, C., Holland, M. M., Large, W. G., Lawrence, D., Lenaerts, J., Lindsay, K., Lipscomb, W., Lofverstrom, M., Mills, M. J., Neale, R., Oleson, K., Otto-Bleisner, B., Phillips, A., Sacks, W., Tilmes, S., Vertenstein, M., Bertini, A., Deser, C., Fox-Kemper, B., Kay, J. E., Kushner, P., Long, M. C., Mickelson, S., Moore, J. K., Nienhouse, E., Polvani, L., Rasch, P. J., Strand, W. G.: The Community Earth System Model version 2 (CESM2), in review at JAMES.

Devine, J. D., Sigurdsson, H., Davis, A. N. and Self, S.: Estimates of sulfur and chlorine yield to the atmosphere from volcanic eruptions and potential climatic effects, J. Geophys. Res. Solid Earth, 89(B7), 6309–6325, doi:10.1029/JB089iB07p06309, 1984.

Drexler, J. W., Rose, W. I., Sparks, R. S. J. and Ledbetter, M. T.: The Los Chocoyos Ash, guatemala: A major stratigraphic marker in middle America and in three ocean basins, Quat. Res., 13(3), 327–345, doi:10.1016/0033-5894(80)90061-7, 1980.

Emile-Geay, J., Seager, R., Cane, M. A., Cook, E. R. and Haug, G. H.: Volcanoes and ENSO over the past millennium, J. Clim., 21(13), 3134–3148, doi:10.1175/2007JCLI1884.1, 2008.

English, J. M., Toon, O. B. and Mills, M. J.: Microphysical simulations of large volcanic eruptions: Pinatubo and Toba, J. Geophys. Res. Atmos., 118(4), 1880–1895, doi:10.1002/jgrd.50196, 2013.

Fierstein, J. and Nathenson, M.: Another look at the calculation of fallout tephra volumes, Bull. Volcanol., 54(2), 156–167, doi:10.1007/BF00278005, 1992.

Fisher, R. A., Wieder, W. R., Sanderson, B. M., Koven, C. D., Oleson, K. W., Xu, C., Fisher, J. B., Shi, M., Walker, A. P. and Lawrence, D. M.: Parametric Controls on Vegetation Responses to Biogeochemical Forcing in the CLM5, J. Adv. Model. Earth Syst., 2019MS001609, doi:10.1029/2019MS001609, 2019.

Gettelman, A., Mills, M. J., Kinnison, D. E., Garcia, R. R., Smith, A. K., Marsh, D. R., Tilmes, S., Vitt, F., Bardeen, C. G., McInerney, J., Liu, H. L., Solomon, S. C., Polvani, L. M., Emmons, L. K., Lamarque, J. F., Richter, J. H., Glanville, A. S., Bacmeister, J. T., Phillips, A. S., Neale, R. B., Simpson, I. R., DuVivier, A. K., Hodzic, A. and Randel, W. J.: The Whole Atmosphere Community Climate Model Version 6 (WACCM6), J. Geophys. Res. Atmos., 6, 2019JD030943, doi:10.1029/2019jd030943, 2019.

von Glasow, R., Bobrowski, N. and Kern, C.: The effects of volcanic eruptions on atmospheric chemistry, Chem. Geol., 263(1–4), 131–142, doi:10.1016/j.chemgeo.2008.08.020, 2009.

Handler, P.: Possible association of stratospheric aerosols and El Nino type events, Geophys. Res. Lett., 11(11), 1121–1124, doi:10.1029/GL011i011p01121, 1984.

Haslam, M. and Petraglia, M.: Comment on "Environmental impact of the 73ka Toba super-eruption in South Asia" by M.A.J. Williams, S.H. Ambrose, S. van der Kaars, C. Ruehlemann, U. Chattopadhyaya, J. Pal and P.R. Chauhan [Palaeogeography, Palaeoclimatology, Palaeoecology 284 (2009) 295, Palaeogeogr. Palaeoclimatol. Palaeoecol., 296(1–2), 199–203, doi:10.1016/j.palaeo.2010.03.057, 2010.

Iles, C. E., Hegerl, G. C., Schurer, A. P. and Zhang, X.: The effect of volcanic eruptions on global precipitation, J. Geophys. Res. Atmos., 118(16), 8770–8786, doi:10.1002/jgrd.50678, 2013.

Jones, G. S., Gregory, J. M., Stott, P. A., Tett, S. F. B. and Thorpe, R. B.: An AOGCM simulation of the climate response to a volcanic super-eruption, Clim. Dyn., 25(7–8), 725–738, doi:10.1007/s00382-005-0066-8, 2005.

Khodri, M., Izumo, T., Vialard, J., Janicot, S., Cassou, C., Lengaigne, M., Mignot, J., Gastineau, G., Guilyardi, E., Lebas, N., Robock, A. and McPhaden, M. J.: Tropical explosive volcanic eruptions can trigger El Ninõ by cooling tropical Africa, Nat. Commun., 8(1), 778, doi:10.1038/s41467-017-00755-6, 2017.

Klobas, J. E., Wilmouth, D. M., Weisenstein, D. K., Anderson, J. G. and Salawitch, R. J.: Ozone depletion following future volcanic eruptions, Geophys. Res. Lett., 44(14), 7490–7499, doi:10.1002/2017GL073972, 2017.

Krüger, K., Kutterolf, S. and Hansteen, T. H.: Halogen release from Plinian eruptions and depletion of stratospheric ozone, in Volcanism and Global Environmental Change, edited by A. Schmidt, K. E. Fristad, and L. T. Elkins-Tanton, pp. 244–259, Cambridge University Press, Cambridge., 2015.

Kutterolf, S., Freundt, A., Pérez, W., Wehrmann, H. and Schmincke, H.-U.: Late Pleistocene to Holocene temporal succession and magnitudes of highly-explosive volcanic eruptions in west-central Nicaragua, J. Volcanol. Geotherm. Res., 163(1–4), 55–82, doi:10.1016/J.JVOLGEORES.2007.02.006, 2007.

Kutterolf, S., Freundt, A., Peréz, W., Mörz, T., Schacht, U., Wehrmann, H. and Schmincke, H.-U.: Pacific offshore record of plinian arc volcanism in Central America: 1. Along-arc correlations, Geochemistry, Geophys. Geosystems, 9(2), doi:10.1029/2007GC001631, 2008a.

Kutterolf, S., Freundt, A. and Peréz, W.: Pacific offshore record of plinian arc volcanism in Central America: 2. Tephra volumes and erupted masses, Geochemistry, Geophys. Geosystems, 9(2), doi:10.1029/2007GC001791, 2008b.

Kutterolf, S., Hansteen, T. H., Appel, K., Freundt, A., Kruger, K., Perez, W. and Wehrmann, H.: Combined bromine and chlorine release from large explosive volcanic eruptions: A threat to stratospheric ozone?, Geology, 41(6), 707–710, doi:10.1130/G34044.1, 2013.

Kutterolf, S., Hansteen, T. H., Freundt, A., Wehrmann, H., Appel, K., Krüger, K. and Pérez, W.: Bromine and chlorine emissions from Plinian eruptions along the Central American Volcanic Arc: From source to atmosphere, Earth Planet. Sci. Lett., 429, 234–246, doi:10.1016/j.epsl.2015.07.064, 2015.

Kutterolf, S., Schindlbeck, J. C., Anselmetti, F. S., Ariztegui, D., Brenner, M., Curtis, J., Schmid, D., Hodell, D. A., Mueller, A., Pérez, L., Pérez, W., Schwalb, A., Frische, M. and Wang, K.-L.: A 400-ka tephrochronological framework for Central

America from Lake Petén Itzá (Guatemala) sediments, Quat. Sci. Rev., 150, 200–220, doi:10.1016/J.QUASCIREV.2016.08.023, 2016.

Li, J., Xie, S. P., Cook, E. R., Morales, M. S., Christie, D. A., Johnson, N. C., Chen, F., D'Arrigo, R., Fowler, A. M., Gou, X. and Fang, K.: El Niño modulations over the past seven centuries, Nat. Clim. Chang., 3(9), 822–826, doi:10.1038/nclimate1936, 2013.

Liu, X., Ma, P.-L., Wang, H., Tilmes, S., Singh, B., Easter, R. C., Ghan, S. J. and Rasch, P. J.: Description and evaluation of a new four-mode version of the Modal Aerosol Module (MAM4) within version 5.3 of the Community Atmosphere Model, Geosci. Model Dev., 9(2), 505–522, doi:10.5194/gmd-9-505-2016, 2016.

Madronich, S. and Flocke, S.: Theoretical Estimation of Biologically Effective UV Radiation at the Earth's Surface, in Solar Ultraviolet Radiation, edited by C. S. Zerefos and A. F. Bais, pp. 23–48, Springer Berlin Heidelberg, Berlin, Heidelberg., 1997.

Metzner, D., Kutterolf, S., Toohey, M., Timmreck, C., Niemeier, U., Freundt, A. and Krüger, K.: Radiative forcing and climate impact resulting from SO2 injections based on a 200,000-year record of Plinian eruptions along the Central American Volcanic Arc, Int. J. Earth Sci., 103(7), 2063–2079, doi:10.1007/s00531-012-0814-z, 2014.

Miller, G. H., Geirsdóttir, Á., Zhong, Y., Larsen, D. J., Otto-Bliesner, B. L., Holland, M. M., Bailey, D. A., Refsnider, K. A., Lehman, S. J., Southon, J. R., Anderson, C., Björnsson, H. and Thordarson, T.: Abrupt onset of the Little Ice Age triggered by volcanism and sustained by sea-ice/ocean feedbacks, Geophys. Res. Lett., 39(2), doi:10.1029/2011GL050168, 2012.

Mills, M. J., Schmidt, A., Easter, R., Solomon, S., Kinnison, D. E., Ghan, S. J., Neely, R. R., Marsh, D. R., Conley, A., Bardeen, C. G. and Gettelman, A.: Global volcanic aerosol properties derived from emissions, 1990-2014, using CESM1(WACCM), J. Geophys. Res. Atmos., 121(5), 2332–2348, doi:10.1002/2015JD024290, 2016.

Mills, M. J., Richter, J. H., Tilmes, S., Kravitz, B., MacMartin, D. G., Glanville, A. A., Tribbia, J. J., Lamarque, J.-F., Vitt, F., Schmidt, A., Gettelman, A., Hannay, C., Bacmeister, J. T. and Kinnison, D. E.: Radiative and Chemical Response to Interactive Stratospheric Sulfate Aerosols in Fully Coupled CESM1(WACCM), J. Geophys. Res. Atmos., 122(23), 13,061-13,078, doi:10.1002/2017JD027006, 2017.

Muthers, S., Arfeuille, F., Raible, C. C. and Rozanov, E.: The impact of volcanic aerosols on stratospheric ozone and the Northern Hemisphere polar vortex: separating radiative from chemical effects under different climate conditions, Atmos. Chem. Phys. Discuss., 15(10), 14275–14314, doi:10.5194/acpd-15-14275-2015, 2015.

Myhre, G., Shindell, D., Bréon, F.-M., Collins, W. D., Fuglestvedt, J., Huang, J., Koch, D., Lamarque, J.-F., Lee, D., Mendoza, B., Nakajima, T., Robock, A., Stephens, G., Takemura, T. and Zhan, H.: Anthropogenic and natural radiative forcing, in Climate Change 2013 the Physical Science Basis: Working Group I Contribution to the Fifth Assessment Report of the Intergovernmental Panel on Climate Change, vol. 9781107057, edited by Intergovernmental Panel on Climate Change, pp. 659–740, Cambridge University Press, Cambridge., 2013.

Niemeier, U., Timmreck, C. and Krüger, K.: Revisiting the Agung 1963 volcanic forcing – impact of one or two eruptions, Atmos. Chem. Phys. Discuss., 1–18, doi:10.5194/acp-2019-415, 2019.

Ohba, M., Shiogama, H., Yokohata, T. and Watanabe, M.: Impact of Strong Tropical Volcanic Eruptions on ENSO Simulated in a Coupled GCM, J. Clim., 26(14), 5169–5182, doi:10.1175/JCLI-D-12-00471.1, 2013.

Pinto, J. P., Turco, R. P. and Toon, O. B.: Self-limiting physical and chemical effects in volcanic eruption clouds, J. Geophys. Res., 94(D8), 11165, doi:10.1029/JD094iD08p11165, 1989.

Plumb, R. A.: Stratospheric Transport, J. Meteorol. Soc. Japan. Ser. II, 80(4B), 793–809, doi:10.2151/jmsj.80.793, 2002.

Predybaylo, E., Stenchikov, G. L., Wittenberg, A. T. and Zeng, F.: Impacts of a pinatubo-size volcanic eruption on ENSO, J. Geophys. Res., 122(2), 925–947, doi:10.1002/2016JD025796, 2017.

Pyle, D. M.: The thickness, volume and grainsize of tephra fall deposits, Bull. Volcanol., 51(1), 1–15, doi:10.1007/BF01086757, 1989.

Pyle, D. M.: Sizes of Volcanic Eruptions, in The Encyclopedia of Volcanoes, edited by H. Sigurdsson, pp. 263–269, Academic Press., 2013.

Rampino, M. R. and Self, S.: Volcanic winter and accelerated glaciation following the Toba super-eruption, Nature, 359(6390), 50–52, doi:10.1038/359050a0, 1992.

Rampino, M. R. and Self, S.: Climate-volcanism feedback and the toba eruption of ~74,000 years ago, Quat. Res., 40(3), 269–280, doi:10.1006/qres.1993.1081, 1993.

Robock, A.: Volcanic eruptions and climate, Rev. Geophys., 38(2), 191–219, doi:10.1029/1998RG000054, 2000.

Robock, A. and Liu, Y.: The Volcanic Signal in Goddard Institute for Space Studies Three-Dimensional Model Simulations, J. Clim., 7(1), 44–55, doi:10.1175/1520-0442(1994)007<0044:TVSIGI>2.0.CO;2, 1994.

Robock, A., Ammann, C. M., Oman, L., Shindell, D., Levis, S. and Stenchikov, G.: Did the Toba volcanic eruption of ~74 ka B.P. produce widespread glaciation?, J. Geophys. Res. Atmos., 114(10), D10107, doi:10.1029/2008JD011652, 2009.

Seinfeld, J. H. and Pandis, S. N.: Atmospheric chemistry and physics: from air pollution to climate change, John Wiley & Sons., 2016.

Rose, W. I., Conway, F. M., Pullinger, C. R., Deino, A., & McIntosh, W. C.: An improved age framework for late Quaternary silicic eruptions in northern Central America. Bulletin of Volcanology, 61(1–2), 106–120. https://doi.org/10.1007/s004450050266, 1999.

Self, S. and King, A. J.: Petrology and sulfur and chlorine emissions of the 1963 eruption of Gunung Agung, Bali, Indonesia, Bull. Volcanol., 58(4), 263–285, doi:10.1007/s004450050139, 1996.

Solomon, S., Garcia, R. R. and Ravishankara, A. R.: On the role of iodine in ozone depletion, J. Geophys. Res., 99(D10), 20491, doi:10.1029/94JD02028, 1994.

Solomon, S.: Stratospheric ozone depletion: A review of concepts and history, Rev. Geophys., 37(3), 275, doi:10.1029/1999RG900008, 1999.

Stenchikov, G., Delworth, T. L., Ramaswamy, V., Stouffer, R. J., Wittenberg, A. and Zeng, F.: Volcanic signals in oceans, J. Geophys. Res., 114(D16), D16104, doi:10.1029/2008JD011673, 2009.

Stevenson, S., Otto-Bliesner, B., Fasullo, J. and Brady, E.: "El Niño Like" hydroclimate responses to last millennium volcanic eruptions, J. Clim., 29(8), 2907–2921, doi:10.1175/JCLI-D-15-0239.1, 2016.

Stevenson, S., Fasullo, J. T., Otto-Bliesner, B. L., Tomas, R. A. and Gao, C.: Role of eruption season in reconciling model and proxy responses to tropical volcanism, Proc. Natl. Acad. Sci., 114(8), 1822–1826, doi:10.1073/pnas.1612505114, 2017.

Svensson, A., Bigler, M., Blunier, T., Clausen, H. B., Dahl-Jensen, D., Fischer, H., Fujita, S., Goto-Azuma, K., Johnsen, S. J., Kawamura, K., Kipfstuhl, S., Kohno, M., Parrenin, F., Popp, T., Rasmussen, S. O., Schwander, J., Seierstad, I., Severi, M., Steffensen, J. P., Udisti, R., Uemura, R., Vallelonga, P., Vinther, B. M., Wegner, A., Wilhelms, F. and Winstrup, M.: Direct linking of Greenland and Antarctic ice cores at the Toba eruption (74 ka BP), Clim. Past, 9(2), 749–766, doi:10.5194/cp-9-749-2013, 2013.

Timmreck, C., Graf, H.-F. F. and Steil, B.: Aerosol Chemistry Interactions After the Mt. Pinatubo Eruption, in Volcanism and the Earth's Atmosphere, vol. 139, pp. 213–225, American Geophysical Union (AGU)., 2003.

Timmreck, C., Graf, H.-F., Lorenz, S. J., Niemeier, U., Zanchettin, D., Matei, D., Jungclaus, J. H. and Crowley, T. J.: Aerosol size confines climate response to volcanic super-eruptions, Geophys. Res. Lett., 37(24), doi:10.1029/2010GL045464, 2010.

Timmreck, C., Graf, H. F., Zanchettin, D., Hagemann, S., Kleinen, T. and Krüger, K.: Climate response to the Toba super-eruption: Regional changes, Quat. Int., 258, 30–44, doi:10.1016/j.quaint.2011.10.008, 2012.

Timmreck, C., Mann, G. W., Aquila, V., Hommel, R., Lee, L. A., Schmidt, A., Brühl, C., Carn, S., Chin, M., Dhomse, S. S., Diehl, T., English, J. M., Mills, M. J., Neely, R., Sheng, J., Toohey, M. and Weisenstein, D.: The Interactive Stratospheric Aerosol Model Intercomparison Project (ISA-MIP): motivation and experimental design, Geosci. Model Dev., 11(7), 2581–2608, doi:10.5194/gmd-11-2581-2018, 2018.

Toohey, M., Krüger, K. and Timmreck, C.: Volcanic sulfate deposition to Greenland and Antarctica: A modeling sensitivity study, J. Geophys. Res. Atmos., 118(10), 4788–4800, doi:10.1002/jgrd.50428, 2013.

Vidal, C. M., Métrich, N., Komorowski, J.-C., Pratomo, I., Michel, A., Kartadinata, N., Robert, V. and Lavigne, F.: The 1257 Samalas eruption (Lombok, Indonesia): the single greatest stratospheric gas release of the Common Era, Sci. Rep., 6(October), 34868, doi:10.1038/srep34868, 2016.

Williams, M. A. J., Ambrose, S. H., van der Kaars, S., Ruehlemann, C., Chattopadhyaya, U., Pal, J. and Chauhan, P. R.: Environmental impact of the 73 ka Toba super-eruption in South Asia, Palaeogeogr. Palaeoclimatol. Palaeoecol., 284(3–4), 295–314, doi:10.1016/j.palaeo.2009.10.009, 2009.

WMO: Scientific Assessment of Ozone Depletion: 2014, Geneva, Switzerland., 2014.

WMO: Scientific Assessment of Ozone Depletion: 2018, Geneva, Switzerland., 2018.

Zanchettin, D., Timmreck, C., Graf, H. F., Rubino, A., Lorenz, S., Lohmann, K., Krüger, K. and Jungclaus, J. H.: Bi-decadal variability excited in the coupled ocean-atmosphere system by strong tropical volcanic eruptions, Clim. Dyn., 39(1–2), 419–444, doi:10.1007/s00382-011-1167-1, 2012.

Zanchettin, D., Khodri, M., Timmreck, C., Toohey, M., Schmidt, A., Gerber, E. P., Hegerl, G., Robock, A., Pausata, F. S. R., Ball, W. T., Bauer, S. E., Bekki, S., Dhomse, S. S., LeGrande, A. N., Mann, G. W., Marshall, L., Mills, M., Marchand, M., Niemeier, U., Poulain, V., Rozanov, E., Rubino, A., Stenke, A., Tsigaridis, K. and Tummon, F.: The Model Intercomparison Project on the climatic response to Volcanic forcing (VolMIP): experimental design and forcing input data for CMIP6, Geosci. Model Dev., 9(8), 2701–2719, doi:10.5194/gmd-9-2701-2016, 2016.

Zhong, Y., Miller, G. H., Otto-Bliesner, B. L., Holland, M. M., Bailey, D. A., Schneider, D. P. and Geirsdottir, A.: Centennial-scale climate change from decadally-paced explosive volcanism: a coupled sea ice-ocean mechanism, Clim. Dyn., 37(11–12), 2373–2387, doi:10.1007/s00382-010-0967-z, 2011.

Zielinski, G. A., Mayewski, P. A., Meeker, L. D., Whitlow, S., Twickler, M. S. and Taylor, K.: Potential atmospheric impact of the Toba mega-eruption ~71,000 years ago, Geophys. Res. Lett., 23(8), 837–840, doi:10.1029/96GL00706, 1996.

Tables

Ensemble name	Number of ensemble members	Branch years	Initial QBO state at 30 hPa	Initial ENSO state (ONI)	Length [years]	Injected sulfur [Mt]	Injected chlorine [Mt]	Injected bromine [Mt]
CTR	1	-	-	-	70	-	-	-
LCY_full	6	3 5 7 8 13 20	E E E W W W	Neutral La Niña El Niño El Niño La Niña Neutral	35	523	120	0.2
LCY_sulf	2	3, 20	E,W	Neutral	35	523	0	0
LCY_1%sulf	1	3	E	Neutral	10	5.23	0	0
LCY_1%halog	1	3	E	Neutral	35	523	12	0.02

Table 1: Summary of model experiments. The injected volatile mass to the stratosphere is based on the total erupted masses of 523 Mt sulfur, 1200 Mt chlorine and 2 Mt bromine applying different injection efficiencies (see Section 2. Methods).

Figures

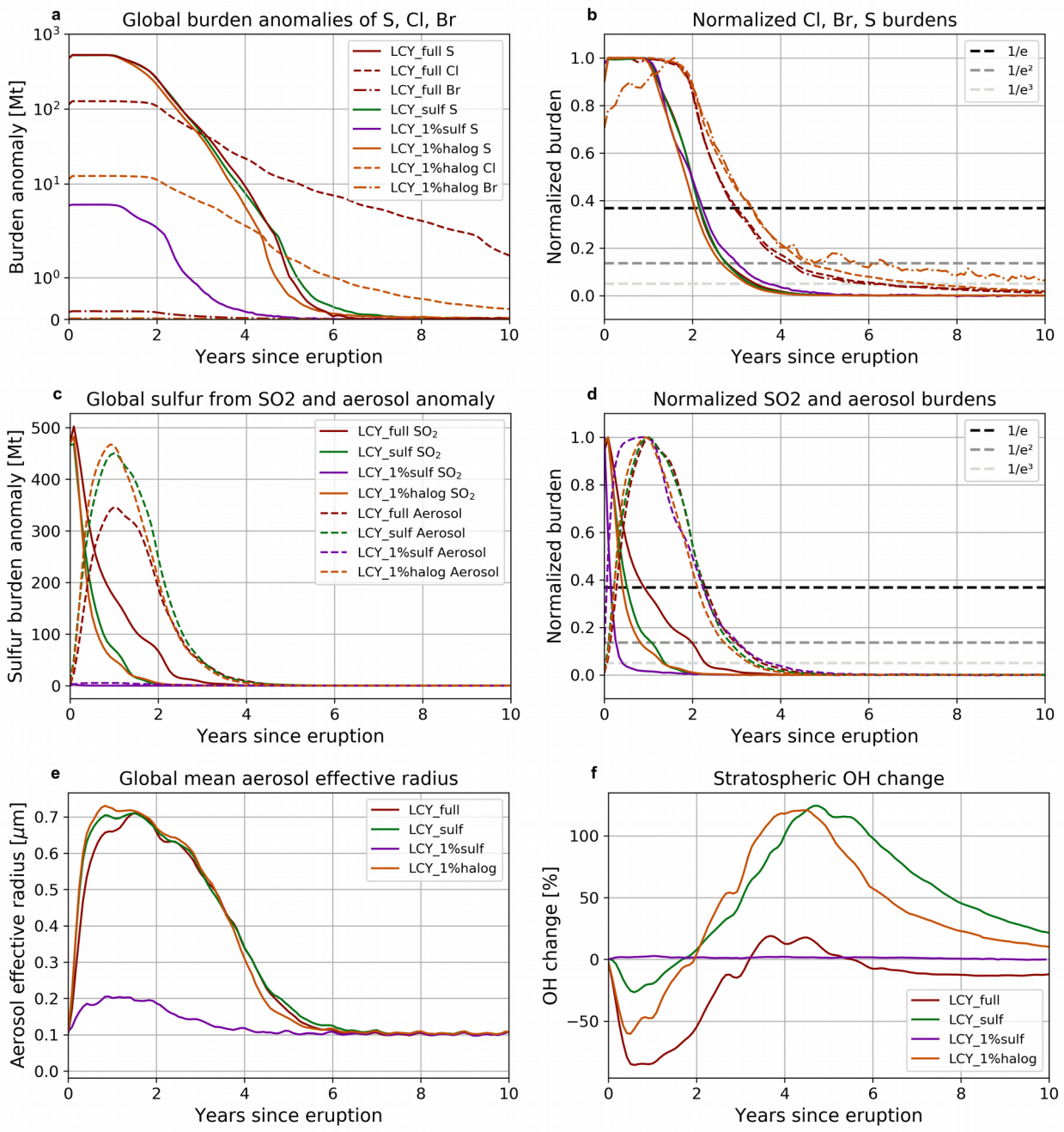

Figure 1: Global evolution of sulfur, halogens, aerosols and OH for the Los Chocoyos simulations. (a) Total sulfur and halogen burden anomalies. (b) Normalized sulfur and halogen burdens. (c) SO_2 and sulfate aerosols burdens. (d) Same as (b) but for SO_2

and sulfate aerosol burdens. (e) Global mean aerosol effective radius. (f) Time evolution of stratospheric OH change relative to CTR. Dashed horizontal lines in b) and d) represents 1/e, $1/e^2$ and $1/e^3$.

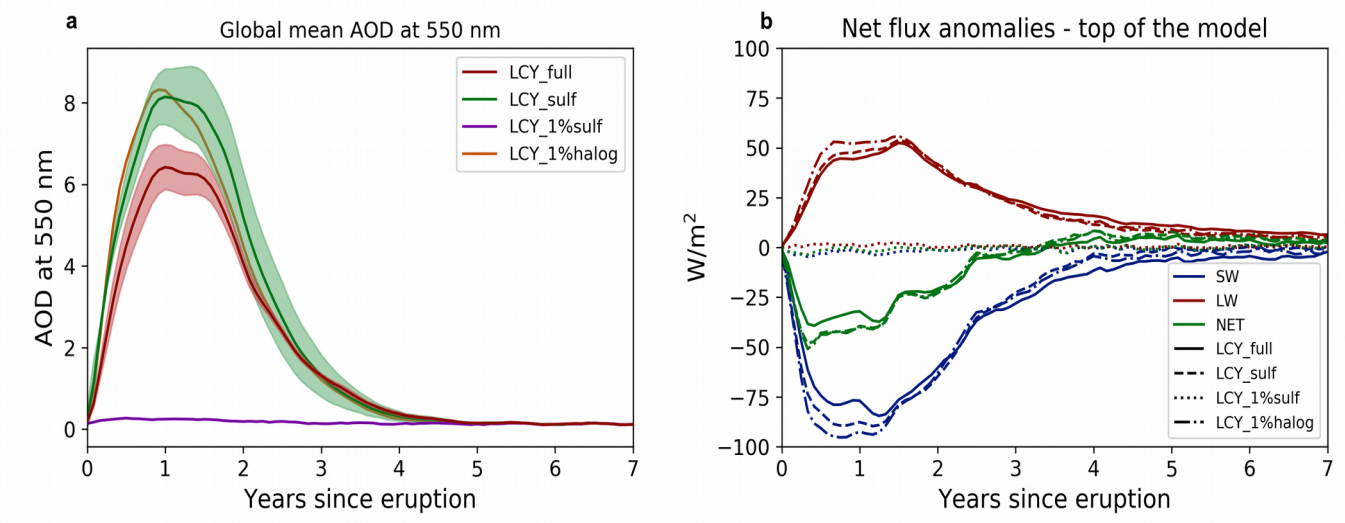

Figure 2: Total aerosol optical depth (AOD) at 550 nm and net radiative flux anomalies at the top of the model in the four LCY eruption scenarios.

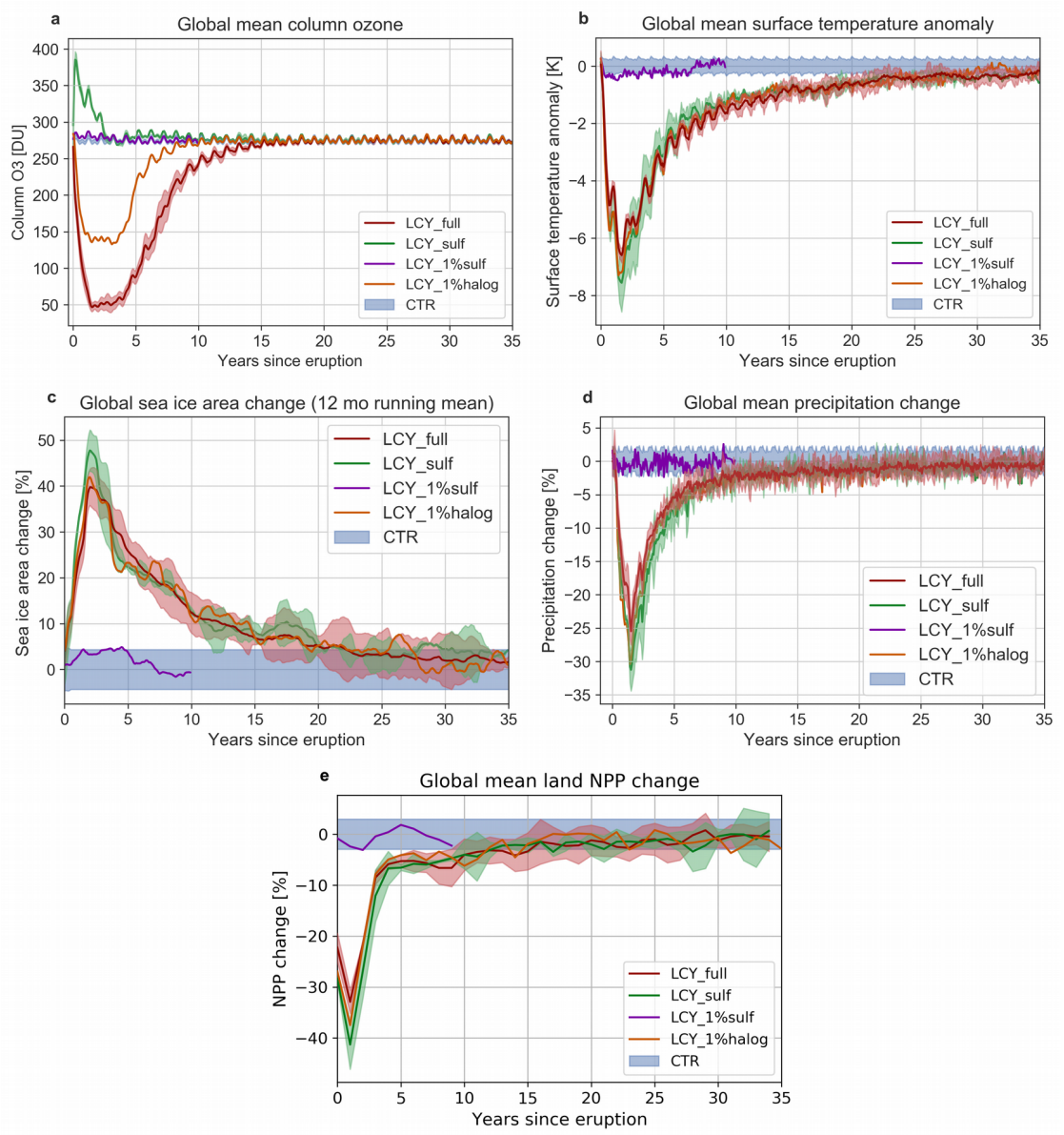

Figure 3: Global mean time-series of column ozone (a) surface temperature anomalies (b), sea ice area change (c), precipitation change (d) and annual mean net primary production (NPP) change (e) in the LCY simulation scenarios.

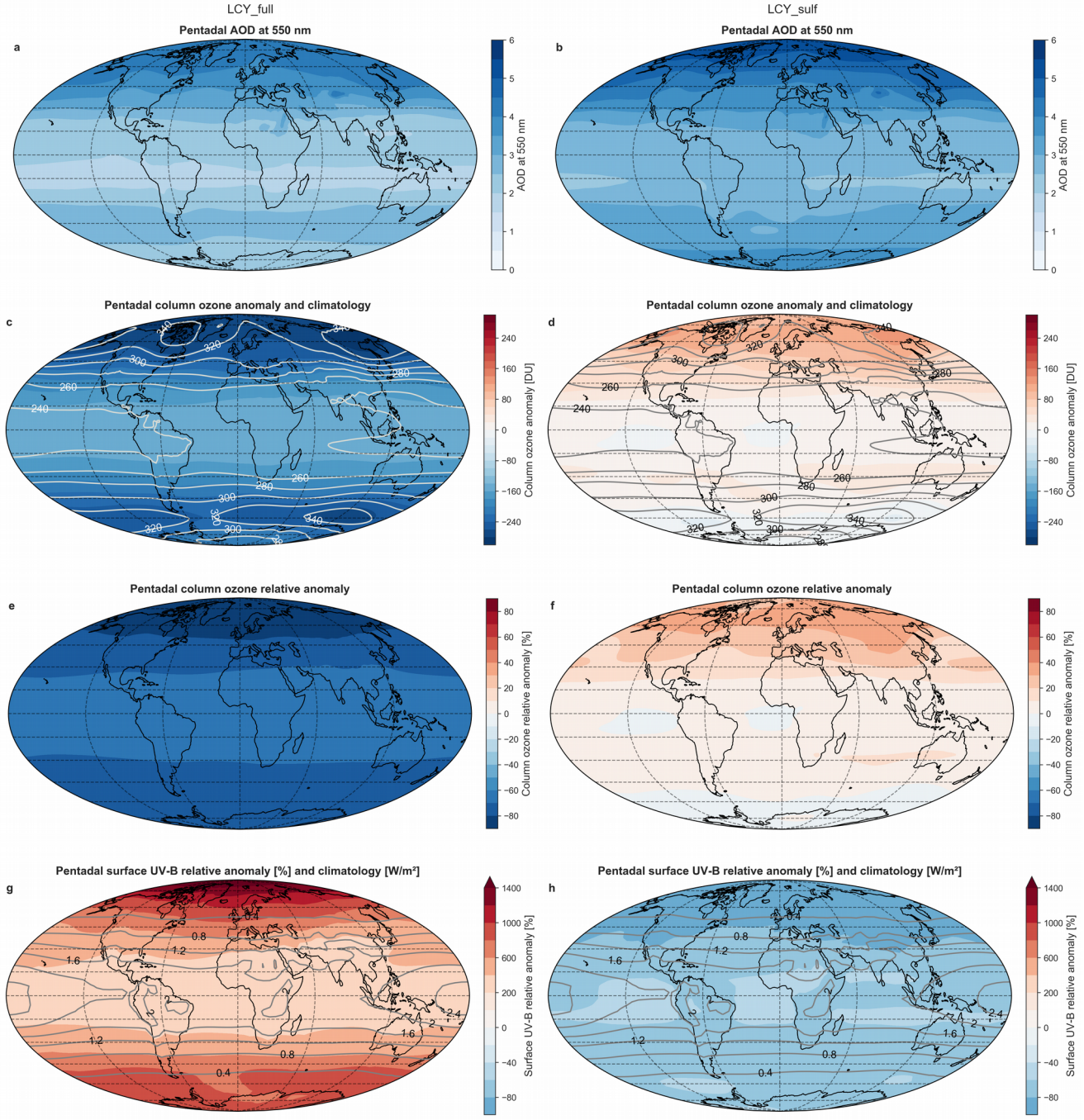

Figure 4: Maps of post-eruption five year (pentadal) means: AOD (a,b), ozone anomaly and climatology (c,d), ozone change (e,f) and surface UV-B weighted for DNA damage change and climatology (g,h) for left side LCY_full (a,c,e,g) and right side LCY_sulf (b,d,f,h).

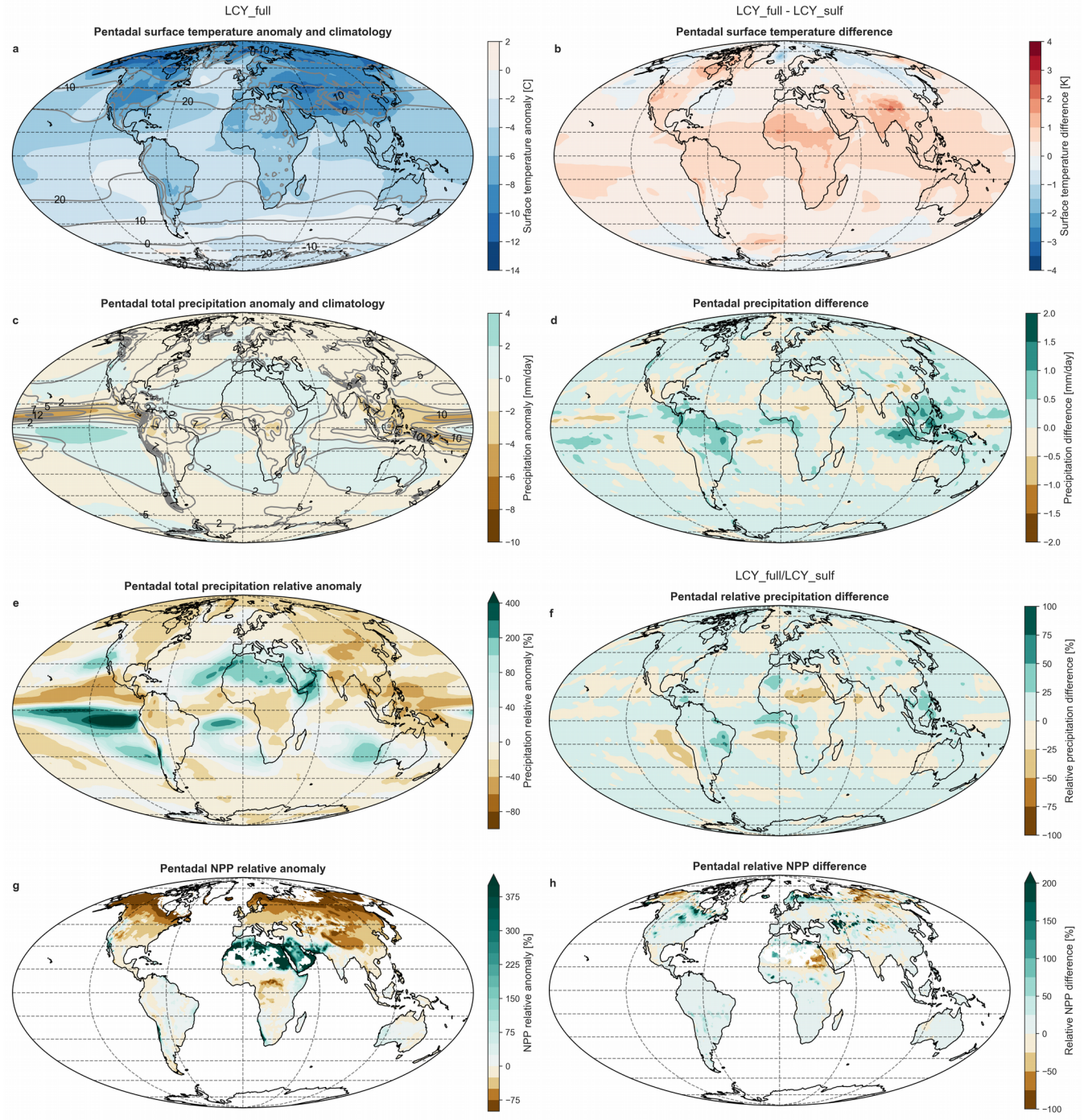

Figure 5: Maps of post-eruption five year (pentadal) means for LCY_full with climatology (a, c, e, g) and the difference between LCY_full and LCY_sulf (b, d, f, h): surface temperature anomaly (a,b), precipitation anomaly (c,d), relative precipitation anomaly (e,f) and relative NPP anomaly (g,h). White areas on the NPP maps indicates invalid values.

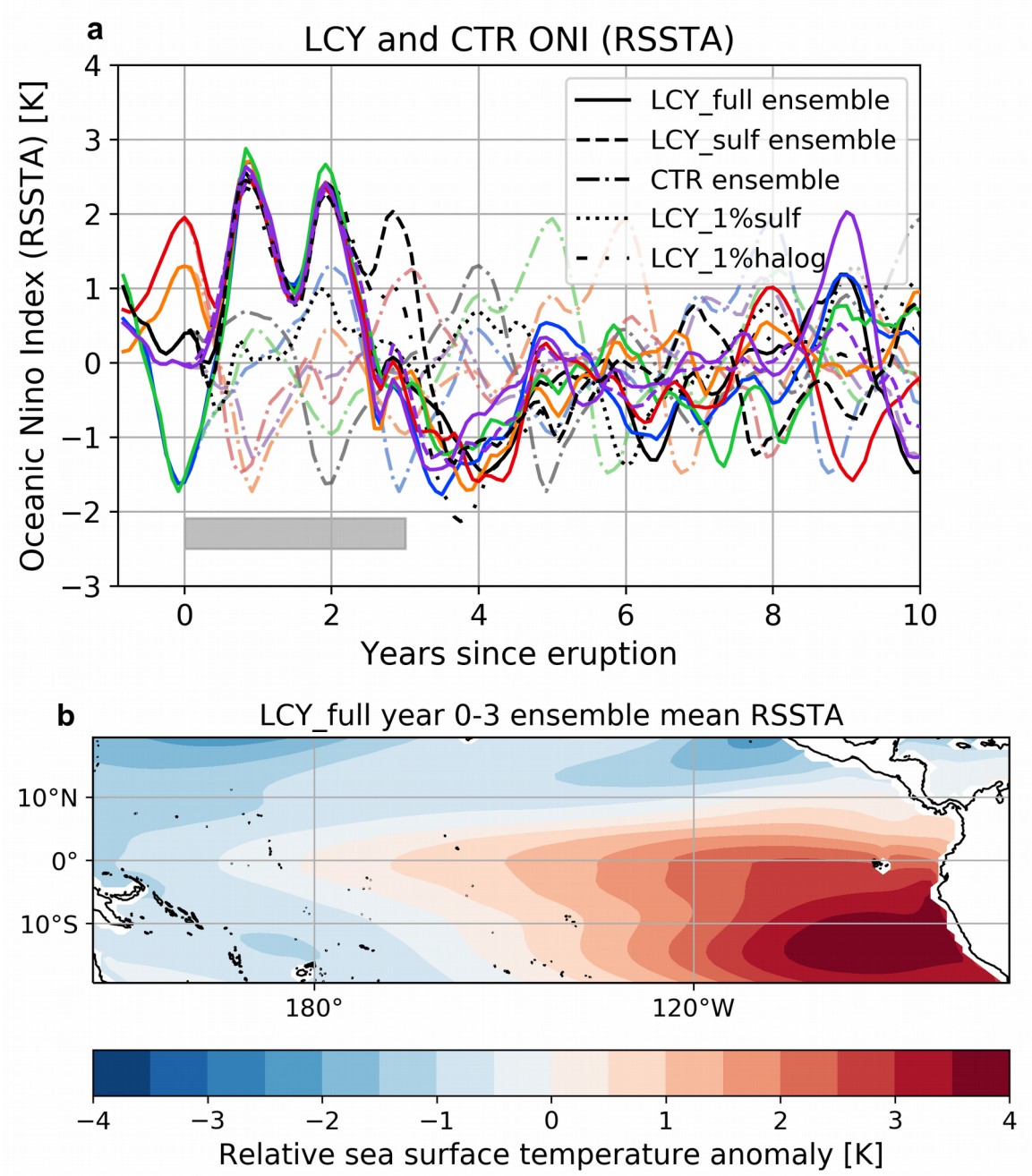

Figure 6: ENSO response to the simulated Los Chocoyos eruption and control run (CTR). (a) Ocean Niño Index (ONI) time series based on relative sea surface temperature anomalies (RSSTA) for the LCY_full ensemble, LCY_sulf and LCY_1%sulf (see legend) in full colour. The corresponding model years of the CTR without an eruption (see branch years in Table 1) are indicated with pale colours. (b) Averaged RSSTA over the equatorial Pacific for the first three post-eruption years as indicated by the grey box in (a).

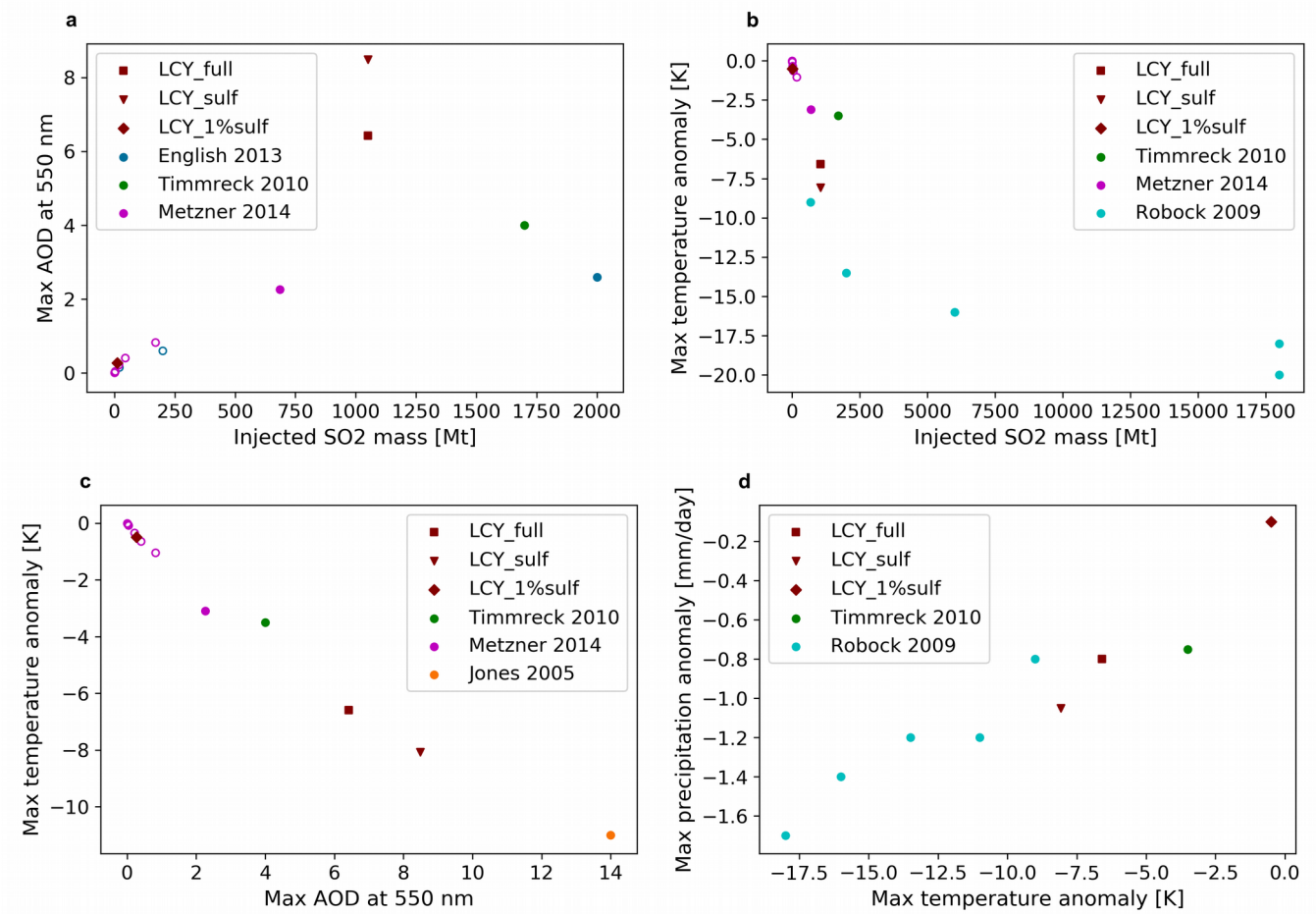

Figure 7: Scatter plots comparing our Los Chocoyos simulations to other super-size volcanic eruption simulations from Jones et al. (2005), Robock et al. (2009), Timmreck et al. (2010), English et al. (2013) and Metzner et al. (2014). Large to extremely large explosive eruptions not classified as super-eruptions are marked with open circles.